Instanton-induced effects in QCD high-energy scattering

Edward Shuryak and Ismail Zahed
Department of Physics and Astronomy, State University of New York, Stony Brook, New York 11794-3800
(Received 30 May 2000; published 26 September 2000)

We evaluate a number of new instanton-induced phenomena in QCD, starting with static dipole-dipole potentials, and proceeding to quark-quark and dipole-dipole scattering at high energy. We use a nonperturbative formulation of the scattering amplitude in terms of a correlator of two Wilson lines (quarks) or Wilson loops (dipoles) and analyze the Euclidean amplitudes with both perturbative gluons and instantons. The results are analytically continued to Minkowski geometry by interpreting the angle between the Wilson lines as rapidity. We discuss the relevance of our results for the phenomenology of near-forward hadronic processes at high energy, especially for processes with multiple color exchanges.

PACS number(s): 12.38.Lg

I. INTRODUCTION

Significant progress reached in the realm of non-perturbative QCD has been mostly related to approaches based on the Euclidean formulation of the theory: numerical simulations using lattice gauge theory, instantons, monopoles, etc. By now, we know a great deal about the important or even dominant role of instanton-induced effects for correlation functions in a variety of hadronic channels, hadronic wave functions and form factors; for a review see [1]. Unfortunately so far many of those results have not been translated to Minkowski space, a crucial step for understanding hadronic high-energy processes. It is however clear that there must be a very general and direct relationship between the hadronic substructure and the details of high energy reactions. Indeed, the non-perturbative modification of QCD vacuum fields induced by the valence quarks studied in Euclidean space-time should look like parton correlations in the transverse plane in a boosted frame. Many known features of partonic distributions, including spin and flavor of the sea quarks, point to their non-perturbative origin. Many more features (such as *fluctuations* of these cross sections and *correlations* in the parton positions in the transverse plane which we briefly discuss at the end of the paper) are still to be studied in detail.

The first systematic step towards a semi-classical but non-perturbative formulation of high-energy scattering in QCD was suggested by Nachtmann [2], who has related the scattering amplitude to expectations of pairs of Wilson lines. Semi-classical expressions with a similar pair of Wilson lines for deep inelastic scattering (DIS) structure functions were also proposed by Muller [3]: in contrast with their traditional interpretation as partonic densities, they were treated as cross sections for targets penetrated by small dipole-like probes at high energy. One systematic way to use these semi-classical expressions is to go back to the perturbative domain and try to improve on the diagrammatic approaches [such as the celebrated Balitskiĭ-Fadin-Kuraev-Lipatov (BFKL) [4] re-summation]: see e.g. calculations of the anomalous dimension of the cross-singularity between two Wilson lines [5] or the analysis of the path exponents in [6].

The approach we will follow in this paper is different: the Wilson lines in question are evaluated semi-classically using instantons. In order to be able to do so, one should start in Euclidean space-time, where those solutions are the saddle points of the functional integrals. The results are then analytically continued back to Minkowski space. Although it was not done before in this form, there are similar approaches in the perturbative context (e.g. [7] and references therein). Another methodically close approach to our analysis is [8,9] where recent progress on the non-perturbative dynamics in $N=4$ super Yang-Mills (SYM) theory was used. In particular, the AdS conformal field theory (CFT) correspondence has been used to evaluate the partonic cross section geometrically, using a deformed string in the curved anti–de Sitter space.

The instanton-induced processes to be considered in this work are either *elastic* scattering of partons or *quasi-elastic* ones, with color transfer between them. They are very different from (and should not be confused with) multi-quanta production processes originally discussed in electroweak theory [10] in connection with baryon number violation and later in QCD in connection to DIS [11]. Such phenomena, associated with small-size instantons, are easier to evaluate and also they should lead to much more spectacular events. However, those lead to much smaller cross sections in comparison to the processes to be discussed below.

In this paper, we will not aim at a development of a realistic model for high-energy hadronic reactions based on instanton physics. Instead, we will answer few questions of principle, such as the following: Is it possible to assess non-perturbatively scattering amplitudes using the Euclidean formulation of the theory? How is the analytical continuation enforced on the non-perturbative amplitudes? What is the magnitude of the instanton induced effects in comparison to the perturbative effects in the scattering of near-forward high energy partons?

In Sec. II we review the perturbative effects on the dipole-dipole potential, including the derivation of a renormalization group solution that can be tested using QCD lattice simulations. In Sec. III we extend the perturbative analysis in Euclidean space to the case of scattering between two quarks and two dipoles. Particular issues regarding the analytical continuation of the perturbative results to Minkowski space are discussed. In Sec. IV, we discuss the effects of instantons on the static potentials for quarks and dipoles. At large dis-

tances the results resemble perturbation theory apart from the large classical enhancement of $(8\pi^2/g^2)^2 \approx 10^2$, which is partially compensated by the diluteness factor $n_0\rho_0^4 \approx (1/3)^4$ [12] of the instantons in the vacuum. In Sec. V, we calculate the scattering amplitudes for quarks and dipoles in the one-instanton approximation. The color preserving part of the amplitude is real and vanishes at high energy. The color exchange part is real but finite at high energy, thereby contributing to the near-forward inelastic scattering or rescattering of partons. In Sec. VI, we extend our discussion to two instantons. We found that for two quarks the cross section is of the order of $\sigma_{qq} \sim (n_0\rho_0^4)^2\rho_0^2$, while for two dipoles it is further suppressed $\sigma_{dd} \sim \sigma_{qq}(d_1^2 d_2^2/\rho_0^4)$. These results are supported by our calculations. In Sec. VII, we discuss the possible role of instantons in cross-section fluctuations. Our conclusions and recommendations are in Sec. VIII.

II. PERTURBATIVE ANALYSIS OF POTENTIALS

A. Dipole-dipole potential

We start with the simplest analysis in Euclidean space, in which the perturbative expansion of two Euclidean Wilson lines leads to the well-known result for the potential between static charges. Indeed, by expanding two Wilson lines to first order in the gauge coupling g, using the Euclidean propagator $\langle A(x)A(y)\rangle \sim 1/(x-y)^2$ with x,y located on two parallel but straight lines, and finally integrating over the relative time $x_0 - y_0$, we readily obtain the Coulomb potential $V(R) \sim \alpha_s(R)/R$.

Now, consider the case of the interaction between two *color neutral* objects, such as *two static color dipoles*. The simplest perturbative process in this case includes double photon-gluon exchange. The problem was solved in QED by Casimir and Polder [13], who have shown that the potential at large distances R is

$$V(R) = -\frac{\alpha_1 \alpha_2}{R^7} \tag{1}$$

where the *polarizabilities* $\alpha_{1,2}$ are of the order of $\alpha_{1,2} \sim \tau_0 d^2$, d is the dipole size and τ_0 is some characteristic time (see below). This result differs from the van der Waals potential $1/R^6$ (valid at smaller R) because of the time delay effects. These observations were generalized to perturbative QCD in [14,15].

The Euclidean approach leads to the 7th power of R in a simple way, provided that the following conditions are satisfied: (i) $d_{1,2} \ll R$ which justifies the dipole approximation and identifies the relevant field operators $(\vec{d}\cdot\vec{E})^2$; (ii) *both* exchanged photons (or gluons) are emitted and absorbed at close x_0 and y_0 times. As a result, the perturbative field correlator $\langle E^2(x)E^2(y)\rangle \sim 1/(x-y)^8 = 1/(R^2+\tau^2)^4$, once integrated over the relative time $\tau = x_0 - y_0$, leads the result $1/R^7$.

The condition (ii) can be understood for complex systems like atoms or hadrons in the following way: the first dipole emission excites the system from (usually an S-wave) ground state to (usually a P-wave) excited state, while the second dipole emission returns the system back. The energies of the intermediate state sets the characteristic lifetime $\tau_0 \approx 1/(E_P - E_S)$.

However, for *static* dipoles the situation is different in QED and QCD. In QED the emission times of two exchanged quanta are independent, but in QCD they are not. Even a *static* dipole can change its color degrees of freedom. Because different total color states of the dipole have different energies, thanks to the Coulomb interaction, we again have excited intermediate states. Therefore the characteristic time is determined by the difference in Coulomb energy between the singlet and octet states:

$$1/\tau_0 = \Delta E = (3\alpha_s/2)/d. \tag{2}$$

Although the dipoles may be *small* $d \ll R$, this time may still be long because in the perturbative domain the coupling constant is small $g^2(d) \ll 1$. As a result, there are two different regimes, when the distance R is large (i) $R \gg \tau_0$ or small (ii) $R \ll \tau_0$. In the former case again the power is 7 and the polarizability is[1] $\alpha = 4\pi d^3/3$. The latter case is the van der Walls domain.

B. RGE analysis of the dipole-dipole potential

On general grounds, the potential between two interacting dipoles can be shown to obey the following equation:

$$\alpha_s \frac{\partial \mathcal{V}(b)}{\partial \alpha_s} = -\frac{1}{2}\int d^3x \,\langle \mathrm{Tr}\, F^2(x)\rangle_b \tag{3}$$

where α_s is the QCD running coupling and the averaging in Eq. (3) is carried in the presence of the two static dipoles a distance b apart. Generically,

$$\mathcal{V}(b) \equiv \mathcal{V}(b,a,\mu,\alpha_s) \approx \mu\,(\mu a)^\kappa F(\mu b, \alpha_s) \tag{4}$$

where μ is the renormalization scale. Hence,

$$\frac{\partial \mathcal{V}}{\partial \alpha_s} = -\frac{1}{\beta}\left((\kappa+1)\,\mathcal{V} + b\frac{\partial \mathcal{V}}{\partial b}\right) \tag{5}$$

where $\beta = d\alpha_s/d\ln\mu$ is the QCD beta function. Inserting Eq. (5) into Eq. (3) yields

$$(\kappa+1)\,\mathcal{V} + b\frac{\partial \mathcal{V}}{\partial b} = \frac{\beta}{2\alpha_s}\int d^3x\,\langle \mathrm{Tr}\, F^2(x)\rangle_b, \tag{6}$$

which is the renormalization group equation (RGE) satisfied by the dipole-dipole potential. At large separations we may assume the dipole-dipole potential in quenched QCD to follow like a power law, i.e.

$$\mathcal{V}(b) \approx \mu\,(\mu a)^\kappa (\mu b)^\gamma, \tag{7}$$

turning Eq. (6) into an algebraic equation

[1] Amusingly, the result is just the volume of a sphere of radius d, from which the perturbative coupling constant g dropped out.

$$(1+\gamma+\kappa)\,\mathcal{V}(b)=\frac{\beta}{2\alpha_s}\int d^3x\,\langle \mathrm{Tr}\,F^2(x)\rangle_b\,. \tag{8}$$

Alternatively, the potential between two dipoles is a measure of the energy density in the presence of two dipoles:

$$\mathcal{V}(b)=\int d^3x\,\langle \Theta_{00}(x)\rangle_b\,. \tag{9}$$

The combination of the RGE (8) and the definition (9) yields a constraint between the exponents κ and γ in Eq. (7) asymptotically, namely

$$\gamma=-1-\kappa+\frac{\beta}{\alpha_s}\frac{1-R}{1+R} \tag{10}$$

with

$$R=\frac{\int d^3x\langle B^2(x)\rangle_b}{\int d^3x\langle E^2(x)\rangle_b} \tag{11}$$

a measure of the magnetic-to-electric ratio in the configuration composed of two static dipoles a distance b away from each other. For a self-dual field $R=1$ and $\gamma=-1-\kappa$ if the asymptotic (7) is assumed.

III. PERTURBATIVE SCATTERING IN EUCLIDEAN GEOMETRY

A. Quark-quark scattering

Generically, we will refer to quark-quark scattering as

$$Q_A(p_1)+Q_B(p_2)\to Q_C(k_1)+Q_D(k_2). \tag{12}$$

We denote by AB and CD, respectively, the incoming and outgoing color and spin of the quarks (polarization for gluons). Using the eikonal approximation and Lehmann-Symanzik-Zimmermann (LSZ) reduction, the scattering amplitude $\mathcal{T}$ for quark-quark scattering reads [2,5,16]

$$\mathcal{T}_{AB,CD}(s,t)\approx -2is\int d^2b\; e^{iq_\perp\cdot b} \times\langle[\mathbf{W}_1(b)-\mathbf{1}]_{AC}[\mathbf{W}_2(0)-\mathbf{1}]_{BD}\rangle \tag{13}$$

where as usual $s=(p_1+p_2)^2$, $t=(p_1-k_1)^2$, $s+t+u=4m^2$ and

$$\mathbf{W}_{1,2}(b)=\mathbf{P}_c\exp\left(ig\int_{-\infty}^{+\infty}d\tau\,A(b+v_{1,2}\tau)\cdot v_{1,2}\right). \tag{14}$$

The 2-dimensional integral in Eq. (13) is over the impact parameter b with $t=-q_\perp^2$, and the averaging is over the gauge configurations using the QCD action. The color bearing amplitude (13) allows for scattering into a singlet or an octet configuration, i.e.

$$\mathcal{T}=\mathcal{T}_1\;\mathbf{1}\otimes\mathbf{1}+\mathcal{T}_{N_c^2-1}\;(\tau^a\otimes\tau^a), \tag{15}$$

following the decomposition $N_c\otimes N_c=1\oplus(N_c^2-1)$. For gluon-gluon scattering the lines are doubled in color space (adjoint representation) and further gauge-invariant contractions are possible. For quark-quark scattering the singlet exchange in the t channel is 0^+ (Pomeron) while for quark-antiquark scattering it is 0^- (odderon) as the two differ by charge conjugation.

A quark with large momentum p travels on a straight line with 4-velocity $\dot{x}=v=p/m$ and $v^2=1$. In the eikonal approximation an ordinary quark transmutes to a scalar quark. The argument applies to any charged particle in a background gluon field, with the following amendments: for antiquarks the 4-velocity v is reversed in the Wilson line and for gluons the Wilson lines are in the adjoint representation. Quark-quark scattering can be also extended to quark-antiquark, gluon-gluon or scalar-scalar scattering. For quark-antiquark scattering the elastic amplitude dominates at large $\sqrt{s}$ since the annihilation part is down by $\sqrt{-t/s}$.

It can be described in Minkowski geometry in the c.m. frame with $p_1/m=(\cosh\gamma/2,\sinh\gamma/2,0_\perp)$ and $p_2/m=(\cosh\gamma/2,-\sinh\gamma/2,0_\perp)$ with the rapidity γ defined through $\cosh\gamma/2=\sqrt{s}/2m$. For $s\gg m^2$ the rapidity gap between the receding scatterers becomes large with $\gamma\approx\log(s/m^2)$. The momentum transfer between the scatterers is $q=p_1-k_1$, with $q_0\approx q_3\approx t/\sqrt{s}$ and $q_\perp^2=tu/(s-4m^2)\approx -t$. Hence $q=(0,0,q_\perp)$ with $q^2=-q_\perp^2=t$. Although the partons or dipoles change their velocities after scattering, this change is small for $s\gg -t$. This is the kinematical assumption behind the use of the eikonal approximation.

In Euclidean geometry, the kinematics is fixed by noting that the Lorenz contraction factor translates to

$$\cosh\gamma=\frac{1}{\sqrt{1-v^2}}=\frac{s}{2m^2}-1\to\cos\theta. \tag{16}$$

Scattering at high energy in Minkowski geometry follows from scattering in Euclidean geometry by analytically continuing $\theta\to -i\gamma$ in the regime $\gamma\approx\log(s/m^2)\gg 1$ [7]. It is sufficient to analyze the scattering for $p_1/m=(1,0,0_\perp)$, $p_2/m=(\cos\theta,-\sin\theta,0_\perp)$, $q=(0,0,q_\perp)$ and $b=(0,0,b_\perp)$. The Minkowski scattering amplitude at high energy can be altogether continued to Euclidean geometry through

$$\mathcal{T}_{AB,CD}(\theta,q)\approx 4m^2\sin\theta\int d^2b\; e^{iq_\perp\cdot b} \times\langle[\mathbf{W}(\theta,b)-\mathbf{1}]_{AC}[\mathbf{W}(0,0)-\mathbf{1}]_{BD}\rangle \tag{17}$$

where

$$\mathbf{W}(b,\theta)=\mathbf{P}_c\exp\left(ig\int_\theta d\tau\,A(b+v\tau)\cdot v\right) \tag{18}$$

with $v=p/m$. The line integral in Eq. (18) is over a straight line sloped at an angle θ away from the vertical.

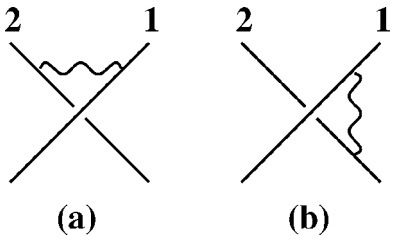

FIG. 1. One-gluon exchange between two receding partons, as discussed in Eq. (19) (a) and Eq. (20) (b).

In QCD perturbation theory, different time-ordering contributions to quark-quark scattering are shown in Fig. 1 to order g^2. They contribute to the T matrix as $\mathcal{T}=2\mathcal{T}_1+2\mathcal{T}_2$ with[2] $(T\to\infty)$

$$\mathcal{T}_1(\theta,b)=\frac{g^2}{4\pi^2}\int_0^T d\tau_1\int_0^T d\tau_2 \times\frac{\cos\theta}{(\tau_1-\tau_2\cos\theta)^2+\tau_2^2\sin^2\theta+b^2} =\frac{\theta}{\tan\theta}\frac{g^2}{4\pi^2}\log\left(\frac{T}{b}\right) \tag{19}$$

and

$$\mathcal{T}_2(\theta,b)=\frac{g^2}{4\pi^2}\int_0^T d\tau_1\int_{-T}^0 d\tau_2 \times\frac{\cos\theta}{(\tau_1-\tau_2\cos\theta)^2+\tau_2^2\sin^2\theta+b^2} =\frac{(\pi-\theta)}{\tan\theta}\frac{g^2}{4\pi^2}\log\left(\frac{T}{b}\right) \tag{20}$$

with $\mathcal{T}_2(\theta,b)=-\mathcal{T}_1(\pi-\theta,b)$ as expected from geometry.[3] We note that the overall linear dependence in θ reflects on the range of the gluon exchanged in rapidity space caused by our ordering in time. This dependence becomes $\theta+(\pi-\theta)=\pi$ in the sum $\mathcal{T}$, i.e.

$$\mathcal{T}(\theta,b)=\frac{g^2}{2\pi^2}\frac{\pi}{\tan\theta}\log\left(\frac{T}{b}\right), \tag{21}$$

as the ordering is unrestricted between 0 and π. All gluons between the spatial distance b and T are also exchanged; hence the infrared sensitivity of the quark-quark scattering amplitude in perturbation theory. This sensitivity drops from the cross section (see below). We note that the order g^2 contribution to Eq. (21) is of order s^0 after analytical continuation, in agreement with the general energy-spin assignment for vector exchange. We recall that the expected behavior is s^{J-1} for a spin-J exchange.

The contribution of Eq. (21) to $\mathcal{T}$ follows after integrating over the impact parameter b. The result in Euclidean geometry is

$$\mathcal{T}(\theta,q)=4m^2\sin\theta\int d^2b\, e^{iq\cdot b}\,\mathcal{T}(\theta,b) =-\cos\theta\frac{g^2}{2}\,\frac{4m^2}{q^2}\int_0^\infty dx\, J_0(x)\log x \tag{22}$$

which can be translated into Minkowski geometry by analytical continuation through $\theta\to -i\gamma$ with $q^2=-t$. In both geometries, $\mathcal{T}$ is purely real and divergent as $t\to 0$, leading to a differential cross section of the order of $d\sigma/dt\approx g^4/t^2$ with a corresponding divergent Coulomb cross section $\sigma\approx g^4/(-t_{min})$. In perturbation theory, the $\mathcal{T}$ matrix acquires absorptive parts and turns complex to higher-order, i.e. $\mathcal{T}=g^2/t+ig^4/t+\cdots$. The Euclidean perturbative analysis can be carried out to higher orders as well, in close analogy with analytically continued Feynman diagrams [7].

B. Dipole-dipole scattering

We now consider dipole-dipole scattering

$$D_A(p_1)+D_B(p_2)\to D_C(k_1)+D_D(k_2) \tag{23}$$

emphasizing its color degrees of freedom. For simplicity we will assume both dipoles to have sizes d, and (in this section) average over their orientations. For pedagogical reasons, we start with a ''naive'' Euclidean approach at large impact parameter b, analogous to the calculation of the dipole-dipole potential above. This would be shown to lead to an incorrect answer for the high energy scattering amplitude. The reason will be given below along with the correct answer.

We will assume that the impact parameter b is large in comparison to the typical time characteristic of the Coulomb interaction inside the dipole, i.e. $b\gg\tau_0\approx d/g^2$. In the elastic dipole-dipole amplitude the dipoles remain color neutral, and we may argue that the leading order is 2-gluon dominated. In analogy to the potential, one may rely on the Coulomb interaction inside the dipole to write the dipole-dipole effective vertex in the form

$$S_{eff}=\alpha_E\int_{-\infty}^{\infty}d\tau\,\dot{x}_\mu\dot{x}_\nu F^a_{\mu\alpha}F^a_{\nu\alpha}(x) \tag{24}$$

where the electric polarizability $\alpha_E\approx(gd)^2/\mathcal{E}$ with $\mathcal{E}\approx g^2/d$ its Rydberg energy [14]. (Higher order operators are suppressed by powers of the dipole size d.)

[2]The color factors can be restored trivially.

[3]The reader may be puzzled by why we are emphasizing this simple point. We note that for more involved multi-gluon processes this cancellation is spoiled by color factors and powers of the angle survive in the answer: after the analytic continuation to Minkowski space these powers become powers of rapidity. They exponentiate and produce powers of the collision energy characteristic of Reggeon behavior (to be described elsewhere).

In leading order in the dipole size, the scattering amplitude then reduces to

$$\mathcal{T}(\theta,b)\approx \alpha_E^2\,\dot{x}_{1\mu}\dot{x}_{1\nu}\dot{x}_{2\lambda}\dot{x}_{2\sigma}\int_{-\infty}^{\infty} d\tau_1\,d\tau_2 \times\langle F^a_{\mu\alpha}F^a_{\nu\alpha}(x_1)\,F^b_{\lambda\beta}F^b_{\sigma\beta}(x_2)\rangle, \qquad (25)$$

with $x_1=v_1\tau_1$ and $x_2=v_2\tau_2+b$. The last expectation value can be unwound using free field theory to obtain

$$\mathcal{T}(\theta,b)\approx \frac{(N_c^2-1)\,\alpha_E^2}{\pi^3\quad b^6}\left(\frac{11}{25}\frac{1}{\sin\theta}+\frac{8}{5}\frac{\cos^2\theta}{\sin\theta}\right). \qquad (26)$$

We note that the result (26) diverges as $\theta\to 0$. For the case $\theta=0$, we obtain the Casimir-Polder-type amplitude

$$\mathcal{T}(0,b)\approx \frac{(N_c^2-1)}{\pi^3}\,\frac{T\alpha_E^2}{b^7}\,\frac{23}{8} \qquad (27)$$

with $T\to\infty$, which differs from the $\theta\neq 0$ by the occurrence of the infrared sensitive factor T/b.

The analytical continuation of Eq. (26) to Minkowski space shows that the first contribution is of order $1/s$, while the second contribution is of order s. This implies that the total cross section is unbound, i.e. $\sigma\sim s$, which is clearly incorrect. Indeed, on physical grounds the total cross section should be constant at large s. In Minkowski space it is easy to understand what went wrong. The electric field of a boosted dipole looks like a Lorenz contracted disk with a very small longitudinal width $b/\cosh y\ll b$. Clearly, at high energy the interaction time of two dipoles is of this order of magnitude, which is much shorter than the Coulomb time τ_0. During this short time, the color rotation induced by the Coulomb interaction can be ignored. Therefore, the use of Eq. (24) in the form of a local 2-gluon exchange is incorrect.[4] This point is actually missed in the Euclidean formulation as the Lorenz factor is $\cos\theta\sim 1$. Although any particular integral can be analytically continued from Euclidean to Minkowski space, kinematical approximations can only be inferred from the Minkowski domain where all parameters have their physical values. This will be understood throughout.

So ignoring the Coulomb interaction and using the eikonal approximation, LSZ reduction and the analytical continuation discussed above, we can write the dipole-dipole scattering amplitude $\mathcal{T}$ in Euclidean geometry similarly to Eq. (17) with

$$\mathbf{W}(\theta,b)=\frac{1}{N_c}\mathrm{Tr}\left[\mathbf{P}_c\exp\left(ig\int_{\mathcal{C}_\theta} d\tau A(x)\cdot v\right)\right] \qquad (28)$$

where x is an element of $\mathcal{C}_\theta$. In Euclidean geometry $\mathcal{C}_\theta$ is a closed rectangular loop of width d, that is sloped at an angle θ with respect to the vertical direction. To leading order in the dipole interaction, $\mathcal{T}$ can be assessed by expanding each Wilson line (28) in powers of g, and treating the resulting 2-gluon correlations perturbatively. The result is

$$\mathcal{T}(\theta,b)\approx \frac{N_c^2-1}{N_c^2}\,\frac{(gd)^4}{32\pi^2}\,\frac{\mathrm{cotan}^2\,\theta}{b^4} \qquad (29)$$

for two identical dipoles $d_1=d_2=d$ with polarizations along the impact parameter b. For small size dipoles, Eq. (29) is the dominant contribution to the scattering amplitude. The analytical continuation shows that cotan $\theta\to -i$, leading to a finite total cross section as expected.

IV. INSTANTON EFFECTS ON THE POTENTIALS

A. Generalities

Instantons are self-dual solutions to the classical Yang-Mills equations in vacuum originally discovered in Ref. [17]. They are classical paths describing tunneling between topologically inequivalent vacua of the gauge theory. In QCD, instantons were argued to be responsible for observable phenomena such as the resolution of the U(1) problem (large η' mass) [18] and the spontaneous breaking of chiral symmetry [12,19]. The interacting instanton liquid model (IILM) has been shown to reproduce multiple correlation functions, including hadronic spectra and coupling constants (for a review see [1]).

Instantons are also commonly used in other gauge theories, especially in supersymmetric gauge theories where supersymmetry makes their effects dominant in the nonperturbative regime. Indeed, some exact results (such as the effective low energy Lagrangian for $N=2$ supersymmetric theories derived by Seiberg and Witten and also the AdS/CFT correspondence suggested by Maldacena[5] for the $N=4$ super-conformal theory) can be exactly reproduced using exclusively the instanton calculus developed in [20].

For the purpose of this paper the topology of instantons is not important: heavy quarks do not interact with fermionic zero modes, and high energy quarks for all purposes behave as heavy quarks. What is important instead is the following technical point: in the instanton field the path-ordered exponents can be evaluated *analytically*, since the color phase rotations take place around the same axis for a fixed path (the instanton is a hedgehog in color-space). The self-duality of the instanton field will also have an effect on some of our results. Once a path-ordered exponent is evaluated in the one-instanton field, the vacuum averages follow through the instanton ensemble average representing the QCD vacuum (dilute phase). This includes averaging over the instanton center position z_μ and size ρ. Specifically, we will use the measure

[4]Note that the result (27) is not based on this approximation, and therefore is still valid.

[5]In fact, the 5-dimensional anti–de Sitter space emerges from the space of the instanton collective coordinates (the center position and size $d^4z\,d\rho/\rho^5$) which will be extensively used for averaging below.

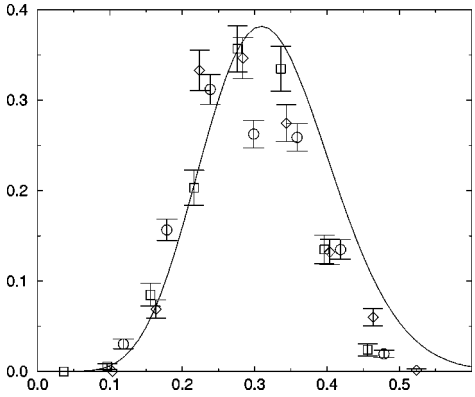

FIG. 2. (a) The instanton density $dn/d\rho d^4z$ [fm^{-5}] versus its size ρ [fm]. (b) The combination $\rho^{-6}dn/d\rho d^4z$, in which the main one-loop behavior drops out for $N_c=3, N_f=0$. The points are from the lattice work [22], for this theory, with $\beta=5.85$ (diamonds), 6.0 (squares) and 6.1 (circles). Their comparison should demonstrate that the results are rather lattice independent. The line corresponds to [21].

$$dn = d\rho\, d^4z\, \frac{D(\rho)}{\rho^5} \tag{30}$$

for both instantons and anti-instantons. The integral over z can be sometimes carried out analytically, but most of the time will be done numerically. The understanding of the instanton size distribution $D(\rho)$ remains an open problem. Naive semi-classical results suggest the [18]

$$D_0(\rho) \approx C_{N_c}\left(\frac{8\pi^2}{g^2(\rho)}\right)^{2N_c} \exp\left(-\frac{8\pi^2}{g^2(\rho)}\right) \approx (\rho\Lambda)^{(11/3)N_c-(2/3)N_f} \tag{31}$$

where C_{N_c} is a constant depending on the number of colors N_c. We have used the asymptotic freedom formula in the exponent to show that this density dramatically grows with the instanton size ρ. However, in the true QCD vacuum instantons and anti-instantons interact with each other and other quantum fields, so that the real function $D(\rho)$ deviates from the semi-classical one for large sizes.

For qualitative estimates we will often use parameters of the instanton liquid model [12], which assumes that all instantons have the same size

$$dn(\rho) = n_0\, d^4z\, d\rho\, \delta(\rho-\rho_0) \tag{32}$$

where n_0 is the total instanton (plus anti-instanton) with a typical radius ρ_0, i.e.

$$n_0 \approx 1 \ \text{fm}^4, \quad \rho_0 \approx 1/3 \ \text{fm}. \tag{33}$$

These values were deduced from phenomenological data extracted from the QCD sum rules, the topological susceptibility and the chiral condensate long before direct lattice data became available. In Fig. 2 we show a sample of such lattice measurements, together with the parametrization for the instanton suppression suggested in [21]. Specifically,

$$dn(\rho) = dn_0(\rho) e^{-2\pi\sigma\rho^2} \tag{34}$$

can be used for averaging in any integral over the instanton density. Typically, the string tension $\sigma \approx (0.440 \ \text{MeV})^2$, so that

$$\langle\rho^2\rangle \approx (0.28 \ \text{fm})^2,$$
$$\langle\rho^4\rangle \approx (0.31 \ \text{fm})^4,$$
$$\langle\rho^5\rangle \approx (0.32 \ \text{fm})^5, \tag{35}$$

which shows that the difference between the realistic averages and simple powers of ρ_0 is relatively small. We will ignore these differences below.

In the analysis to follow, the parameters capturing the instanton physics will appear as two dimensionless quantities: (i) a small *diluteness* parameter and (ii) a large *action* of an instanton (per $\hbar$):

$$n_0\rho_0^4 \approx \left(\frac{1}{3}\right)^4 \quad S_0 = \frac{8\pi^2}{g^2(\rho_0)} \approx (10\text{–}15). \tag{36}$$

The small factor is a penalty for finding the instanton, and the large factor is a classical enhancement relative to perturbation theory. Their interplay would cause particular effects to be parametrically large or small.

B. Static quarks

At the one instanton level, the various potentials for a static quark-antiquark potential have been assessed long ago [23], including the spin-dependent part. We will briefly review this assessment for completeness. We recall that the various components of the potential follow from the rectangular $T\times R$ Wilson loop

$$V(R) = -\frac{1}{T}\lim_{T\to\infty} \ln\langle \mathbf{W}(T,R)\rangle \tag{37}$$

evaluated in a classical instanton field, after averaging over the instanton position. In the Wilson loop, the path-ordered exponents $P\exp(ig\int A_\mu dx_\mu)$ can be evaluated analytically as the instanton locks the color orientation to space. Indeed, the static potentials involve $A_0^a \sim \eta_{0,\nu}^a (x-z)_\nu \sim (x-z)^a$ where $(\vec{x}-\vec{z})$ refers to the distance between the quark position and the 3D coordinate of the instanton center.[6] The resulting color rotation angle α [23] and the unit vector n^a around which the rotation takes place are defined through

$$\mathbf{W} = \exp\left(-i\pi \frac{\tau^a (z_a - r_a)}{[(r_a-z_a)^2+\rho^2]^{1/2}}\right) = \exp(-i\pi\tau^a n_a \alpha). \tag{38}$$

If all relevant distances are comparable, $|r_a - z_a| \sim \rho_0$, the rotation angle is O(1), showing that the expansion in field strength is in general not justified. For a small-size dipole, the potential is small $V(R\to 0) \approx R^2$, since the path-ordered

[6]The time position of the instanton z_4 is irrelevant.

lines in **W** are close enough to cause partial cancellation. However when $R \approx \rho_0$, and both path-ordered lines happen to be on the opposite sides of the instanton center, the color rotations on both lines adds up and the potential becomes roughly linear in R and more sizable. Finally, when the dipole is too large, the potential saturates.[7]

The quark-antiquark potential calculated in [23] can be expressed as

$$V(R) = \int dn(\rho) \rho^3 F(R/\rho) \tag{39}$$

where the dimensionless function F is defined as

$$F = \int \frac{d^3 z}{N_c \rho^3} \mathrm{Tr}(1 - \mathbf{W}_1 \mathbf{W}_2^\dagger). \tag{40}$$

The trace part of the integrand is

$$2(1 - \cos\alpha_1 \cos\alpha_2 - \vec{n}_1 \cdot \vec{n}_2 \sin\alpha_1 \sin\alpha_2) \tag{41}$$

where the angles α_i and vectors n_i^a are defined in Eq. (38). This function is shown in Fig. 3a. In order to emphasize the small-R ''dipole limit'' $V(R) \sim R^2$ (to be important for what follows), we have also plotted the ratio of this function to its dipole limit in Fig. 3b. One can see that the dipole approximation has an unexpectedly large range of applicability: this ratio does not change appreciably (less than 25%) until $R \approx \rho_0$. One may expect a similar accuracy of the dipole approximation in other applications to be discussed.

For large R the potential [23] goes to a constant plus a Coulomb term

$$V(R \to \infty) = 37 \int \frac{d\rho}{\rho^2} D(\rho) - \frac{4\pi^3}{3R} \frac{d\rho}{\rho} D(\rho) + \cdots \tag{42}$$

which can be interpreted as the instanton contribution to the *mass* and *charge* renormalization, respectively. It is instructive to compare the magnitude of the latter to the perturbative potential, through

$$\frac{V_{inst}}{V_{pert}} = \frac{\pi^2}{2} (n_0 \rho_0^4) \left(\frac{8\pi^2}{g^2(\rho_0)} \right), \tag{43}$$

with $V_{pert} = 4\alpha_s/3R$. The ratio is the product of the *diluteness parameter*[8] (the fraction of space-time occupied by instantons) times the *classical enhancement* through the instanton action (per $\hbar$). Using the phenomenological parameters discussed above, we observe that the diluteness is compensated by the classical enhancement, so that the instanton corrections at $R \approx \rho_0$ are actually comparable to the perturbative Coulomb effect.

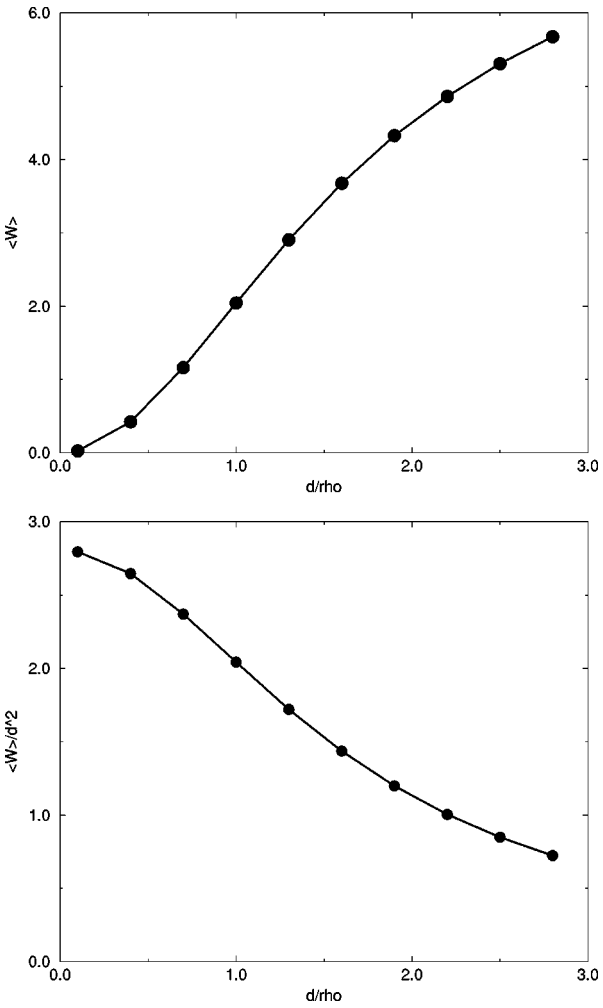

FIG. 3. (a) F as defined in Eq. (39) as a function of the quark-antiquark distance R measured in units of the instanton size ρ_0, (b) the rescaled function $F(R/\rho_0)/R^2$ to exhibit the accuracy of the dipole approximation at small R.

However, instantons are not the only non-perturbative effects contributing to the static quark-antiquark potential. At large R confinement in the form of a QCD string with $V_{conf} \approx \sigma R$ dominates. In fact, already for $R \approx \rho_0 \sim 0.3$ fm confinement is dominant, with the instanton-induced potential accounting for only 10–15 %.[9] For a detailed study of these issues at the multi-instanton level, one can consult Refs. [24] for a numerical analysis and [25] for analytical results.

C. Static dipoles

Unlike the quark-antiquark potential, the dipole-dipole potential is insensitive to confinement, and the instanton-

[7] In Ref. [31] one of us has noticed that this behavior is surprisingly similar to that experimentally observed in deep inelastic scattering, if the Q^2 dependence of structure functions is treated as the dependence of the cross section on the dipole size.

[8] The coefficient in front of $\pi^2 \rho^4/2$ happens to be the volume of a 4-sphere.

[9] The claim made in [26], that instanton effects account for the confining potential, is incorrect.

induced interaction may be easier to identify. In the latter case, we will consider two cases where the characteristic time within the dipole is either (i) *short*, $\tau_0 \sim d/g^2 \ll \rho$, or (ii) *long*, $\tau_0 \gg \rho_0$, in comparison to the instanton size. These two cases translate to a magnitude of the dipole field $A_0 \sim g/d$ which is large (i) or small (ii) in comparison to that of the instanton field $A_\mu \sim 1/g\rho$.

In case (i) the static potential can be written in terms of the polarizabilities and the correlator of gluo-electric fields

$$V(R) = \alpha_1 \alpha_2 \int d\tau \langle \vec{E}^2(\tau, R) \vec{E}^2(0,0) \rangle. \tag{44}$$

This field strength correlator can be evaluated by substituting the expression for the instanton field:

$$\vec{E}^2(x) = \vec{B}^2(x) = \frac{96\rho^4}{g^2} \frac{1}{[(x-z)^2+\rho^2]^4}. \tag{45}$$

The averaging of the correlator over the location of the instanton position z can be carried out analytically [27]:

$$\langle [gG^a_{\mu\nu}(x)]^2 [gG^a_{\mu\nu}(0)]^2 \rangle = \frac{384 g^4}{\pi^4 x^8} + (n_0 \rho_0^4) \Pi_{inst}(x/\rho)/\rho^8, \tag{46}$$

where the last term was added to account for the perturbative contribution. The dimensionless function describing the instanton contribution is

$$\Pi_{inst}(y) = \frac{12288\pi^2}{y^6 (y^2+4)^5} \left(y^8 + 28 y^6 - 94 y^4 - 160 y^2 - 120 + \frac{240}{y\sqrt{y^2+4}} (y^6 + 2y^4 + 3y^2 + 2) \operatorname{arcsinh}(y/2) \right). \tag{47}$$

Its behavior is shown in Fig. 4a. Its ratio to the perturbative contribution to the same correlator (for $g=2$ or $\alpha_s = 0.32$) is shown in Fig. 4b. As expected, it is small at small distances $x \ll \rho_0$. At large distances, the instanton-induced contribution has the same behavior $\Pi_{inst} \approx 1/R^8$ as the perturbative one. Furthermore, the ratio of the two is about 30, much more than the ''instanton-induced charge renormalization'' (43) we discussed in the preceding subsection. About the same is found in the potentials themselves (the correlator integrated over the time difference) as shown in Fig. 4d. The perturbative behavior is dominated by *two* gluons rather than one, and therefore the instanton effect occurs with a classical enhancement *squared*:

$$\frac{V_{inst}}{V_{pert}} \sim (n_0 \rho_0^4) \left(\frac{8\pi^2}{g^2(\rho_0)} \right)^2. \tag{48}$$

This feature implies that instanton effects are much more important for dipole-dipole interactions at $R \approx \rho_0 \approx 0.3$ fm than the perturbative Casimir-Polder effects. We will argue below that this is generic for all processes demanding multi-

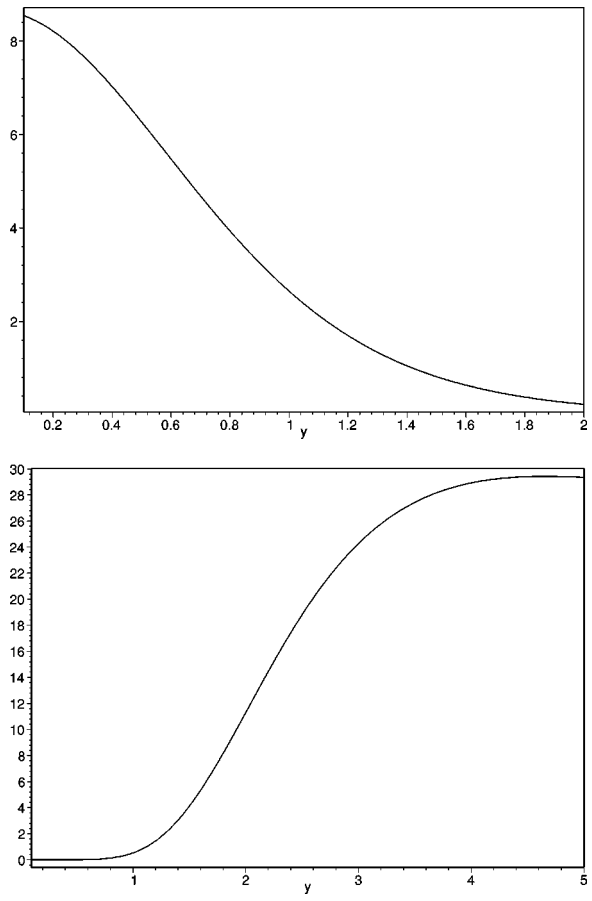

FIG. 4. (a) Field strength correlator Π_{inst} as defined in Eq. (47) versus the distance in units of the instanton size x/ρ_0. (b) Ratio of the instanton-induced term in the correlator to the perturbative one versus the distance.

gluon exchanges, and that instanton-induced processes can become dominant in this case.

In case (ii), the dipoles can be considered quasi-static in time, $\tau_0 \sim d/g^2 \gg \rho_0$, and the time evolution of the color degrees of freedom due to the Coulomb interaction can be ignored. In other words, the dynamics is driven entirely by the instanton field. The potential between two dipoles is now

$$V_{dd}(R) = \int dn(\rho) \rho^3 F_{dd}(R/\rho) \tag{49}$$

with

$$F_{dd} = \int \frac{d^3 z}{N_c \rho^3} (1 - \operatorname{Tr} \mathbf{W}_1 \operatorname{Tr} \mathbf{W}_2). \tag{50}$$

Here $\mathbf{W}$ are rectangular Wilson *loops* for each dipole, traced separately. Averaging over the instanton position can be done numerically. The results are shown in Fig. 5. The outcome is proportional to $d_1^2 d_2^2$ (dipole moments) rather than $\alpha_1 \alpha_2$ (electric polarizabilities), when d is reasonably small in comparison to ρ_0. The large distance potential is a few % that of $V(R) \approx d_1^2 d_2^2 \rho_0^2 / R^7$. Note that it is larger than the

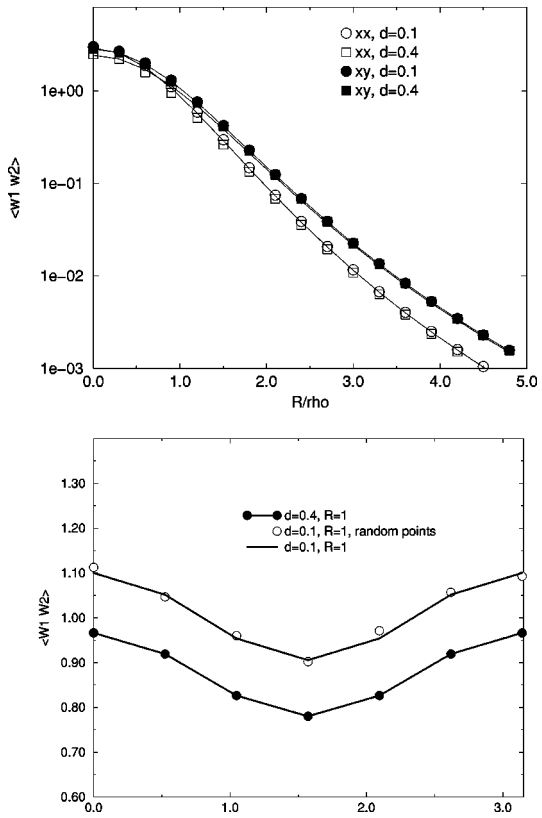

FIG. 5. (a) Two correlated Wilson loops as a function of the distance R between their centers, divided by $d_1^2 d_2^2$ for two dipole sizes, $d_1 = d_2 = 0.1$ (circles) and 0.4 ρ_0 (squares). The agreement between the points shows that the dipole scaling holds well for such sizes. Also two dipole orientations are shown. The open points are for both dipoles oriented in the x direction (the same direction as the distance between them R) while the closed points for the xy orientation. The disagreement between those means that the dipole-dipole forces depend on the orientations. Further details on the orientation dependence are shown in (b). $F_{dd}(R=\rho_0)$ shows the dependence on the orientation angle of one dipole in the x-y plane. The solid points and curves are for a 4D lattice-type integration over the instanton center, and the open points are for the alternative Monte Carlo integration: their spread from the curve shows the magnitude of the uncertainties involved.

perturbative one since ρ_0^2 is assumed to be much larger than $d_1 d_2$, but both answers have the same (zeroth) power of g.

In general the dipole-dipole potential cannot be approximated by the correlator of scalars E^2, as can be checked through its dependence on the relative orientation of the dipoles. Even in the dipole (quadratic) approximations for sufficiently small dipoles ($d_i \ll \rho$) one can define 4 invariant functions for the dipole-dipole interaction

$$V(R) = d_1^i d_1^j d_2^l d_2^m [A(R)\,\delta_{ij}\delta_{lm} + \tfrac{1}{2}B(R)(n^i n^j \delta_{lm} + n^l n^m \delta_{ij}) + C(R) n^i n^l \delta_{jm} + D(R) n^i n^j n^l n^m]. \tag{51}$$

The first function $A(R)$ accounts for the spin-zero gluonic operator $\vec{E}^2$ discussed at the beginning of this subsection. However, as one can see from Fig 5, other functions also contribute. In (a) we compare the xx orientation (or $A+B+C+D$) with the xy one (or $A+B/2$) and see a clear difference. In (b) we note the dependence on the rotation angle for one of the dipoles, which shows a clear $\cos^2\theta$ behavior expected from the expression above.

V. ONE-INSTANTON EFFECT ON SCATTERING

A. Quark-quark scattering

Our first step now is the generalization of Eq. (38) to an arbitrary orientation θ of the Wilson line. The analytical continuation to Minkowski space follows from $\theta \to iy$ with y identified as the rapidity difference between the receding partons. The untraced and tilted Wilson line in the one-instanton background reads

$$\mathbf{W}(\theta, b) = \cos\alpha - i\,\tau\cdot\hat{n}\,\sin\alpha \tag{52}$$

where

$$n^a = \mathbf{R}^{ab}\,\eta^b_{\mu\nu}\dot{x}_\mu (z-b)_\nu = \mathbf{R}^{ab}\,\mathbf{n}^b \tag{53}$$

and $\alpha = \pi\gamma/\sqrt{\gamma^2+\rho^2}$ with

$$\gamma^2 = n\cdot n = \mathbf{n}\cdot\mathbf{n} = (z_4 \sin\theta - z_3\cos\theta)^2 + (b - z_\perp)^2. \tag{54}$$

The one-instanton contribution to the untraced QQ-scattering amplitude follows from the following correlator

$$\langle \mathbf{W}_{AC}(\theta,b)\mathbf{W}_{BD}(0,0)\rangle \approx n_0 \int d^4z \left(\cos\alpha \cos\underline{\alpha}\,\mathbf{1}_{AC}\,\mathbf{1}_{BD} - \frac{1}{N_c^2-1}\hat{\mathbf{n}}\cdot\underline{\hat{\mathbf{n}}}\sin\alpha\sin\underline{\alpha}(\tau^a)_{AC}(\tau^a)_{BD}\right), \tag{55}$$

where the (under)bar notation means the same as the corresponding un-bar notation with $\theta = 0$ and $b = 0$.

Furthermore,

$$\left\langle \frac{1}{N_c}\mathrm{Tr}[\mathbf{W}(\theta,b)\,\mathbf{W}(0,0)]\right\rangle = \frac{2n_0}{N_c}\int d^4z(\cos\alpha\cos\underline{\alpha} - \hat{\mathbf{n}}\cdot\underline{\hat{\mathbf{n}}}\sin\alpha\sin\underline{\alpha}). \tag{56}$$

The integrand in Eq. (56) can be simplified by changing variable $(z_4\sin\theta - z_3\cos\theta) \to z_4$ and dropping the terms that vanish under the z integration. Hence

$$\left\langle \frac{1}{N_c}\mathrm{Tr}[\mathbf{W}(\theta,b)\,\mathbf{W}(0,0)]\right\rangle = \frac{2n_0}{N_c}\int d^4z\left(\frac{1}{\sin\theta}\cos\tilde{\alpha}\cos\underline{\tilde{\alpha}} - \frac{1}{\tan\theta}\sin\tilde{\alpha}\sin\underline{\tilde{\alpha}}\frac{z_\perp^2 - z_\perp\cdot b}{\tilde{\gamma}\,\underline{\tilde{\gamma}}}\right). \tag{57}$$

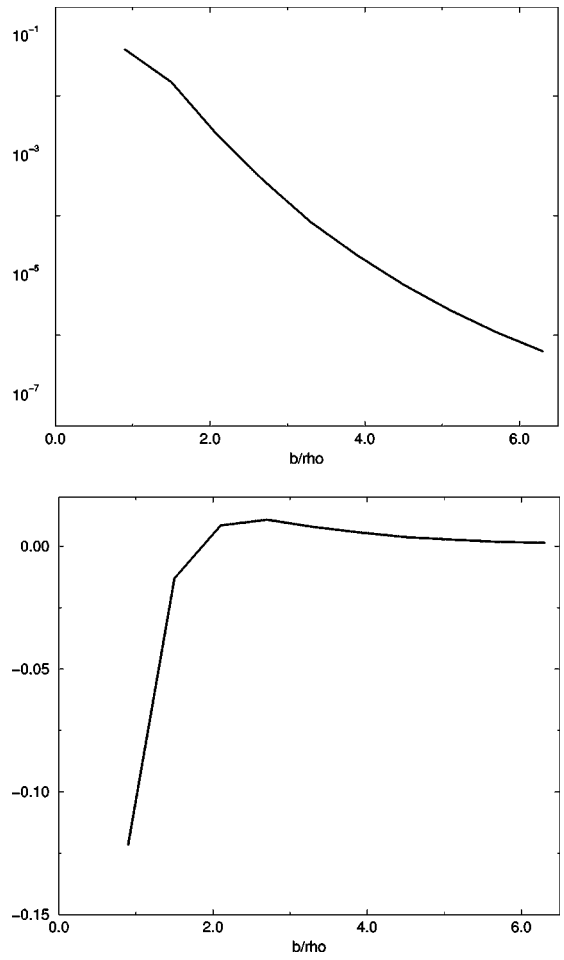

FIG. 6. (a) and (b) show the two functions n_0F_{cc} and n_0F_{ss} defined in Eq. (58) versus the impact parameter b (in units of the instanton radius).

The tilded parameters follow from the un-tilded ones by setting $\theta=\pi/2$. We note that $\tilde{\gamma}=\gamma=|\vec{z}|$. After analytical continuation, the first term produces the elastic amplitude which decays as $1/s$ with the energy. The second term corresponds to the color-changing amplitude. It is of order s^0 and dominates at high energy. Specifically

$$\left\langle \frac{1}{N_c}\mathrm{Tr}[\mathbf{W}(\theta,b)\,\mathbf{W}(0,0)]\right\rangle = \frac{2n_0}{N_c}\left(\frac{1}{\sin\theta}F_{cc}(b/\rho_0)-\frac{1}{\tan\theta}F_{ss}(b/\rho_0)\right). \quad (58)$$

We show in Fig. 6 the numerical behavior of the two contributions in Eq. (58). Note that the second function (which describes color-inelastic collisions and survives in the high energy limit) changes sign, before decreasing to zero at large b. This limit corresponds to the instanton-induced renormalization of the one-gluon exchange, and it has therefore logarithmic behavior in b, as described in Sec. III A.

B. Dipole-dipole and multi-parton scattering

One can directly generalize the calculation of the quark-quark scattering amplitude to that of any number of partons. For that, we assume that they all move with high energy in some reference frame and opposite direction: in Euclidean space those would propagate along two directions, with parton numbers N_1 and N_2 respectively. Any one of them, passing through the instanton field, is rotated in color space by a different angle α_i around a different axis $\vec{n}_i$, depending on the shortest distance between its path and the instanton center. Integration over all possible color orientations of the instanton leads then to global color conservation.

Before discussing specific cases in details, let us make a general qualitative statement about such processes. We have found in the previous section that (the color-changing) quark-quark instanton-induced scattering has a finite high energy limit. For perturbative n-gluon exchange a factor of α_s^n is paid, while for an instanton mediated scattering a factor of $n_0\rho_0^4$ is paid (the price to find the instanton at the right place), no matter how many partons participate. Since the instanton vacuum is dilute, the one-gluon mediated process dominates the instanton one. However, the situation dramatically changes for two or more gluon exchanges: the instanton-induced amplitude is about the same for any number of partons, provided that all of them pass at a distance $\approx\rho_0$ from the instanton center.

Now, consider a dipole configuration of size d chosen in the transverse plane of a $\bar{q}q$ located on a straight line sloped at an angle θ in Euclidean space. Let AA be the initial color of the dipole and CD its final color. The Wilson loop with open color for the dipole configuration in the one-instanton background is

$$\begin{aligned}\mathcal{W}_{AA}^{CD}(\theta,b)=&\cos\alpha_-\cos\alpha_+\,\mathbf{1}_{CD}\\ &+i\cos\alpha_-\sin\alpha_+\mathbf{R}^{ab}\,\hat{\mathbf{n}}_+^b\,(\tau^a)_{DC}\\ &-i\sin\alpha_-\cos\alpha_+\mathbf{R}^{ab}\,\hat{\mathbf{n}}_-^b\,(\tau^a)_{DC}\\ &+\sin\alpha_-\sin\alpha_+\mathbf{R}^{ab}\,\mathbf{R}^{cd}\hat{\mathbf{n}}_-^b\,\hat{\mathbf{n}}_+^d\,(\tau^c\tau^a)_{DC}.\end{aligned} \quad (59)$$

We have defined

$$\alpha_\pm=\frac{\pi\gamma_\pm}{\sqrt{\gamma_\pm+\rho^2}}$$

$$\gamma_\pm^2=(z_4\sin\theta-z_3\cos\theta)^2+\left(z_\perp-b\pm\frac{d}{2}\right)^2$$

$$\mathbf{n}_+\cdot\mathbf{n}_-=\left((z_4\sin\theta-z_3\cos\theta)^2+(b-z_\perp)^2-\frac{d^2}{4}\right) \quad (60)$$

with $\mathbf{n}_\pm\cdot\mathbf{n}_\pm=\gamma_\pm^2$. The scattering amplitude of an initial dipole through an instanton after averaging over the global color orientation $\mathbf{R}$ is

$$\frac{2}{N_c}(\cos\alpha_-\cos\alpha_++\hat{\mathbf{n}}_-\cdot\hat{\mathbf{n}}_+\sin\alpha_-\sin\alpha_+)\,\mathbf{1}_{CD} \quad (61)$$

which reduces to the color-singlet channel. Specifically,

$$\mathcal{W}(\theta,b)=\frac{2}{N_c}(\cos\alpha_-\cos\alpha_+ + \hat{\mathbf{n}}_-\cdot\hat{\mathbf{n}}_+\sin\alpha_-\sin\alpha_+). \tag{62}$$

The θ dependence in Eqs. (61),(62) can be readily eliminated by carrying the integration over the instanton position z through the same change of variable discussed in the quark-quark scattering, resulting in an amplitude that depends only on $1/\sin\theta$. In Minkowski space this translates to $1/s$ which vanishes at high energy. Indeed, the dipole-dipole scattering amplitude through a single instanton is

$$\langle \mathbf{W}(\theta,b)\,\mathbf{W}(0,0)\rangle \approx \frac{n_0}{\sin\theta}\int d^4z\,\tilde{\mathcal{W}}(\theta,b)\tilde{\mathcal{W}}(0,0) \tag{63}$$

where $\tilde{\mathcal{W}}$ follows from $\mathcal{W}$ by setting $\theta=\pi/2$. Note that in this case $\mathcal{W}(0,0)=\tilde{\mathcal{W}}(0,0)$.

It is clear from Eq. (59) that while scattering through an instanton, the dipole has to flip color to keep track of the velocity of the quarks in the dipole. The process is color inelastic and therefore only contributes to the inelastic amplitude to first order in the instanton density n_0 and to the elastic amplitude to second order in the instanton density, a situation reminiscent of one- and two-gluon exchange.

The dipole-dipole scattering amplitude with open-color in the final state can be constructed by using two dipole configurations as given by Eq. (59) with a relative angle θ. After averaging over the instanton color orientations we obtain

$$\mathcal{W}^{CD}_{AA}(\theta,b)\,\mathcal{W}^{C'D'}_{A'A'}(0,0) = \frac{2}{N_c}\mathcal{W}_1\mathbf{1}_{CD}\,\mathbf{1}_{C'D'}+\frac{1}{N_c^2-1}\mathcal{W}_{N_c^2-1}(\tau^a)_{DC}(\tau^a)_{D'C'}, \tag{64}$$

with the singlet part

$$\begin{aligned}\mathcal{W}_1 =& \cos\alpha_-\cos\alpha_+\cos\underline{\alpha}_-\cos\underline{\alpha}_+ \\ &+\mathbf{n}_-\cdot\mathbf{n}_+\underline{\mathbf{n}}_-\cdot\underline{\mathbf{n}}_+\sin\alpha_-\sin\alpha_+\sin\underline{\alpha}_-\sin\underline{\alpha}_+ \\ &+\underline{\mathbf{n}}_-\cdot\underline{\mathbf{n}}_+\cos\alpha_-\cos\alpha_+\sin\underline{\alpha}_-\sin\underline{\alpha}_+ \\ &+\mathbf{n}_-\cdot\mathbf{n}_+\sin\alpha_-\sin\alpha_+\cos\underline{\alpha}_-\cos\underline{\alpha}_+,\end{aligned} \tag{65}$$

and the octet part

$$\begin{aligned}\mathcal{W}_{N_c^2-1} =& -\cos\alpha_-\sin\alpha_+\cos\underline{\alpha}_-\sin\underline{\alpha}_+\mathbf{n}_+\cdot\underline{\mathbf{n}}_+ \\ &-\sin\alpha_-\cos\alpha_+\sin\underline{\alpha}_-\cos\underline{\alpha}_+\mathbf{n}_-\cdot\underline{\mathbf{n}}_- \\ &+\cos\alpha_-\sin\alpha_+\sin\underline{\alpha}_-\cos\underline{\alpha}_+\mathbf{n}_+\cdot\underline{\mathbf{n}}_- \\ &+\sin\alpha_-\cos\alpha_+\cos\underline{\alpha}_-\sin\underline{\alpha}_+\mathbf{n}_-\cdot\underline{\mathbf{n}}_+ \\ &-\sin\alpha_-\sin\alpha_+\sin\underline{\alpha}_-\sin\underline{\alpha}_+ \\ &\times(\mathbf{n}_-\cdot\underline{\mathbf{n}}_-\mathbf{n}_+\cdot\underline{\mathbf{n}}_+-\mathbf{n}_-\cdot\underline{\mathbf{n}}_+\mathbf{n}_+\cdot\underline{\mathbf{n}}_-).\end{aligned} \tag{66}$$

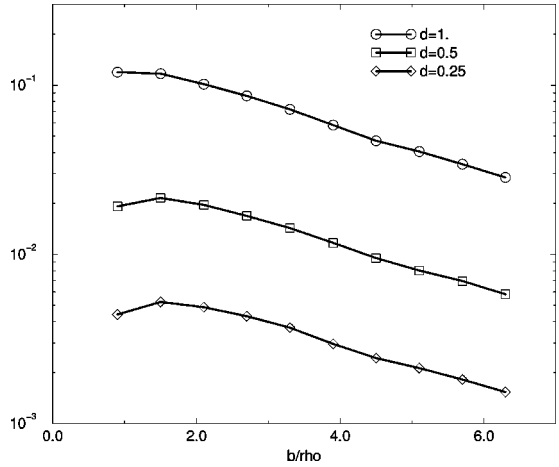

FIG. 7. (a) $F_{N_c^2-1}(b,d)$ defined in Eq. (39) versus the dipole-dipole impact parameter b (in units of the instanton size ρ_0). Each curve corresponds to a different dipole size d (same units).

As in the case of quark-quark scattering, the (color) elastic dipole-dipole amplitude scales as $1/\sin\theta$ and vanishes at high energy after analytical continuation. However, the (color) inelastic part of the amplitude does not. After performing the shift of variables described before, the θ dependence drops from all the angles α. There is a remaining θ dependence in the four combinations $\mathbf{n}\cdot\mathbf{n}$. In general, the θ dependence in the latter is linear in $\sin\theta$ or $\cos\theta$, and one may worry that the last term in Eq. (66) may involve higher powers of the trigonometric functions, which would yield to an unphysical cross section growing as s after analytical continuation. We have checked that this is not the case, since

$$\mathbf{n}_-\cdot\underline{\mathbf{n}}_-\mathbf{n}_+\cdot\underline{\mathbf{n}}_+-\mathbf{n}_-\cdot\underline{\mathbf{n}}_+\mathbf{n}_+\cdot\underline{\mathbf{n}}_-\to d^2(z_2^2-\cos\theta\, z_3 z_4')$$

where z_4' is the new z_4 after the change of variable. Moreover, the $\cos\theta$ term drops in the integral over z (odd under $z_3\to -z_3$), making this contribution to Eq. (66) subleading at high energy after analytical continuation.[10] Finally, we note that all $\sin\theta$ contributions in Eq. (66) drop following similar parity considerations. As a result, the pertinent octet contribution to the scattering amplitude is proportional to cotan θ which is $1/i\tan y=1/iv$ after analytical continuation.

We have assessed numerically the function

$$F_{N_c^2-1}\left(\frac{b}{\rho}_0,\frac{d}{\rho}_0\right)=\frac{n_0}{\cos\theta}\int d^4z\,\mathcal{W}_{N_c^2-1} \tag{67}$$

which is shown in Fig. 7 for different dipole sizes. We find that the dipole approximation scaling $F_{N_c^2-1}\sim d^2$ works well, even for sizes as large as the instanton size $d=\rho_0$.

[10]This cancellation is not generic. Indeed, the square of this contribution would be leading.

VI. TWO-INSTANTON EFFECT

We have shown above that the instanton contribution at large s but small t behaves in a way similar to one-gluon exchange: only color-inelastic channels survive in the high energy limit. This means that the contribution to the total cross section appears in the amplitude squared, leading naturally to the concept of two-instanton exchange. The latter contribution to each Wilson line is more involved. To streamline the discussion we will present the analysis of the two instanton contribution to the differential cross section of quark-quark scattering at high energy. Similar considerations apply to dipole-dipole scattering as we briefly mention at the end of this section. Indeed, for the quark-quark scattering, unitarity implies that the two-instanton contribution to the differential cross section is

$$\frac{d\sigma}{dt}\approx\frac{1}{s^2}\sum_{CD}\ |\mathcal{T}_{AC}^{BD}|^2, \tag{68}$$

with the averaging over the initial colors A,B understood. Inserting Eq. (13) after the substitution (55), we obtain

$$\frac{d\sigma}{dt}\approx\left(\frac{4n_0}{N_c}\right)^2\int db\,db'\,e^{iq\cdot(b-b')}\left(\mathbf{J}+\frac{1}{(N_c^2-1)}\mathbf{K}\right) \tag{69}$$

with

$$\mathbf{J}=\int d^4z\,(\cos\alpha-1)(\cos\underline{\alpha}-1)\int d^4z'(\cos\alpha'-1)\times(\cos\underline{\alpha}'-1)$$

$$\mathbf{K}=\int d^4z\,\hat{\mathbf{n}}\cdot\underline{\hat{\mathbf{n}}}\sin\alpha\sin\underline{\alpha}\int d^4z'\,\hat{\mathbf{n}}'\cdot\underline{\hat{\mathbf{n}}}'\sin\alpha'\sin\underline{\alpha}'. \tag{70}$$

The primed variables follow from the unprimed ones through the substitution $z,b\to z',b'$. For large $\sqrt{s}$, $\mathbf{J}\approx(1-F_{cc})(1-F'_{cc})/s^2$,[11] and $\mathbf{K}=F_{ss}F'_{ss}$, so that

$$\frac{d\sigma}{dt}\approx\frac{16n_0^2}{N_c^2(N_c^2-1)}\left|\int db\,e^{iq\cdot b}F_{ss}\left(\frac{b}{\rho_0}\right)\right|^2. \tag{71}$$

In particular, the forward scattering amplitude in the two-instanton approximation is

$$\sigma(t=0)\approx\frac{16n_0^2}{N_c^2(N_c^2-1)}\int_0^\infty dq_\perp^2\left|\int db\,e^{iq\cdot b}F_{ss}\left(\frac{b}{\rho_0}\right)\right|^2, \tag{72}$$

which is finite at large $\sqrt{s}$. Hence, for forward scattering partons in the instanton vacuum model, we have

$$\sigma_{qq}\approx(n_0\rho_0^4)^2\rho_0^2. \tag{73}$$

[11]Up to self-energies.

Clearly, the present analysis generalizes to the dipole-dipole scattering amplitude by using Eq. (64) instead of Eq. (55) and proceeding as before. The outcome is a finite scattering cross section

$$\sigma(t=0)\approx\frac{4n_0^2}{(N_c^2-1)}\int_0^\infty dq_\perp^2\left|\int db\,e^{iq\cdot b}F_{N_c^2-1}\left(\frac{b}{\rho_0},\frac{d}{\rho_0}\right)\right|^2. \tag{74}$$

Generically, the dipole-dipole cross section relates to the quark-quark cross section in the forward direction through

$$\sigma_{dd}\approx\sigma_{qq}\frac{(d_1d_2)^2}{\rho_0^4}. \tag{75}$$

It is instructive to compare our instanton results to those developed by Dosch and collaborators [28] in the context of the stochastic vacuum model (SVM). In brief, in the SVM model the Wilson lines are expanded in powers of the field strength using a non-Abelian form of the Stokes theorem in the Gaussian approximation. A typical hadronic cross section in the SVM is

$$\sigma\approx\langle(gG)^2\rangle^2a^{10}\mathbf{F}(R_h/a) \tag{76}$$

where the first factor is the ''gluon condensate,'' a is a fitted correlation length, and $\mathbf{F}$ is some dimensionless function depending on the hadronic radius R_h. Although our assumptions and those of [28] are very different regarding the character of the vacuum state, it is amusing to note the agreement between Eqs. (75) and (76). Indeed, the correlation length a of the SVM model is related (and in fact numerically close) to our instanton radius $\rho_0\approx1/3$ fm, while the gluon condensate $\langle(gG)^2\rangle$ of the SVM is simply proportional to the instanton density n_0 in the instanton model.

The most significant difference between these two approaches apart from their dynamical content and the way we have carried the analytical continuation is the fact that we do not expand in field strength. In fact, in the instanton model there is no parameter which would allow to do so for strong instanton fields. This difference is rather important as it is on it that our conclusion regarding multiple color exchanges is based. [In the SVM with Wick-theorem-like decomposition, those would be just products of single exchanges, like in perturbative QCD (PQCD).]

VII. CROSS SECTION FLUCTUATIONS

So far, we have considered the *average* value of the cross section for a parton in a state of unit probability. However, partons and, in general, hadrons are complex quantum mechanical states.[12] Hence, the quantum system is characterized by some amplitude of probability through its wave function, and its corresponding scattering cross section is proba-

[12]A truly elementary particle may have only one state and non-fluctuating cross section: it may have diffraction but no inelastic diffraction.

bilistic with a *probability distribution* $P(\sigma)$. This idea was originally suggested by Good and Walker [29], who emphasized that inelastic diffraction is a way to quantify this distribution via the second moment $\Delta\sigma^2=\langle(\sigma^2-\langle\sigma\rangle)^2\rangle$.

The extraction of this and the next (cubic) moment for the pion and the nucleon using available data was carried out years later [30], allowing for a reconstruction of the distribution $P(\sigma)$. A striking aspect of these results is that the nucleon fluctuations are large and comparable to the pion fluctuations. This outcome does not fit with the constituent quark model where the pion is a 2-body system, and the nucleon is a 3-body system, with more degrees of freedom. One of us [31] had already noticed that this can be a further indication for strongly correlated scalar diquarks in a nucleon. An experimental test for this idea is to measure cross section fluctuations for a decuplet baryon such as Ω^-. In the latter there are no diquarks, and smaller fluctuations (typical of a 3-body state) are expected. Another aspect of these fluctuations worth mentioning here is that they seem to be maximal for $\sqrt{s}\approx 100$ GeV, decreasing at very large energies. It supports well the idea that the ''most fluctuating'' partons are at $x\sim 10^{-2}$, while at much smaller x one basically approaches a non-fluctuating black disk.

Although in the present paper we have limited our discussion to issues of methodology, it is worth pointing out that the present concept of fluctuations in cross sections can be used to discriminate between the instanton effects herein described and other descriptions based either on perturbative multi-gluon exchange or non-perturbative vacuum structures.

Indeed, the standard multi-photon exchange in QED leads to an (eikonalized) exponential scattering amplitude, with Poisson-like fluctuations. If the mean number of quanta exchanged $\langle n\rangle\gg 1$ (e.g. for heavy ions with large $Z\approx 1/\alpha$), the distribution becomes narrow and we approach a classical limit, with weakly fluctuating scattering. Modulo color factors, the same conclusion applies to multi-gluon exchange in QCD. In contrast, the instanton-induced effects have completely different statistical properties. The field of the instanton itself is classical, hence coherent. However, the distribution over the instanton size and position is quantum (in contrast to the Coulomb field of the ion just mentioned), thereby leading to cross section fluctuations. The latter are further enhanced by the *diluteness* of the instanton ensemble: the quark may appear very black, provided a tunneling event happens to be close to it, and rather transparent otherwise. As noticed already in [12], quarks are ''twinkling'' objects, as the associated gauge and quark fields are strongly fluctuating.

To quantify some of these statements we show in Fig. 8 how such a distribution looks. We plot $|F_{ss}(b=1)|^2$, at fixed impact parameter $b=\rho_0$. The distribution corresponds to instantons being homogeneously distributed in the 4D sphere around the center of the collision point, with a radius $R_s\approx 2.2\rho_0$ such that $\pi^2R_s^4/2=1/n_0$ or in a smaller sphere within $R<\rho_0$. However, the resulting amplitude is highly inhomogeneous, with a large peak at small amplitude and a long tail at large amplitude. Comparing the solid and dashed curves, one can see that the latter is due to instantons sitting near the center of the system.

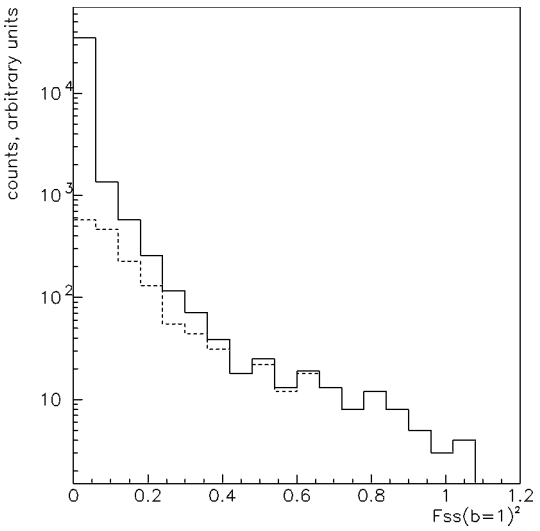

FIG. 8. The distribution $|F_{ss}(b=\rho_0)|^2$ with instantons filling homogeneously the 4D ''Wigner-Seitz sphere'' of radius $2.2\rho_0$ (solid histogram) or the smaller sphere of radius $1.0\rho_0$ (dashed histogram).

VIII. CONCLUSIONS AND OUTLOOK

A. Conclusions

Several new instanton-generated phenomena have been studied in this work: static potentials for color dipoles, and high energy quark-quark and dipole-dipole scattering. The nature of the instanton effects makes their contribution to these processes different from the contribution expected in perturbation theory.

Overall, the magnitude of the instanton contribution is governed by two competing factors: (i) a diluteness factor $n_0\rho_0^4\ll 1$, reflecting the fact that their density in the QCD vacuum is small ($n_0\rho_0^4\ll 1$), and (ii) a classical enhancement factor, the instanton action of which is large ($S_0/\hbar\approx 10\gg 1$). Naturally, the more partons are involved in a particular process, the more powers of α_s appear in the perturbative result for a particular process. This penalty does not apply to the instanton contribution. One way to quantify this difference is to note that the ratio of the instanton-to-perturbative contributions contains a power of the classical enhancement parameter, and this power grows with the number of partons involved. Typically the first power due to the classical instanton enhancement cannot really compensate for the small diluteness of the instantons in the vacuum. However, the second power is already sufficient to make the instanton effects larger than the perturbative ones as we have now established for the potentials. Indeed, the dipole-dipole instanton-induced potential exceeds significantly (by a factor of ~ 25) the perturbative contribution for distances $R>\rho_0$.

Based on these ideas, we have extended the analysis to near-forward parton-parton scattering amplitudes, treating in detail the case of quark-quark and dipole-dipole scattering. The key to our analysis was the concept of analytical continuation in the rapidity variable, which we have applied to both the perturbative and instanton analysis for comparison.

In the perturbative analysis, one- and two-gluon exchanges differ fundamentally in the sense that the former is color changing (inelastic), while the latter is color preserving (elastic). Indeed, the two-gluon exchange mechanism [32] constitutes the starting ground for the soft Pomeron approach to dipole-dipole scattering. Since the instantons can be viewed as multi-gluon configurations (classical fields), we have suggested that they maybe a viable starting point to analyze soft parton-parton scatterings. We have shown that the instanton-induced amplitudes involve also color-elastic and color-inelastic channels. After analytical continuation, the one-instanton contribution to the color-elastic channel is purely real and vanishes as $1/\sqrt{s}$ (much like a scalar exchange). In other words, in this work a single instanton is not ''cut'' and its multi-gluon content is not used. Instantons contribute to soft parton-parton scattering like the *t*-channel gluons mostly through color exchange channels or through re-scattering in the elastic channel. The leading instanton contribution involves a two-instanton-prong channel, and yields a finite elastic parton-parton scattering amplitude after analytical continuation in rapidity space. Our result is reminiscent of the one reached in the stochastic vacuum model [28], although our assumptions and methodology are different.

B. Outlook

The results we have derived were achieved in Euclidean space prior to our pertinent analytical continuation. Therefore, they are testable from first principles by repeating our analysis using instead lattice QCD simulations. Indeed, the non-perturbative dipole-dipole forces could be studied. In contrast to the quark-antiquark potential and to the best of our knowledge, those forces have not been investigated on the lattice. Also, the various scattering amplitudes discussed in the present work can and should be looked at, leading to multi-parton amplitudes as we have qualitatively discussed. Note that not only can the potentials and scattering amplitudes themselves be derived, but the degree of their correlation with the presence of instantons in the underlying configurations can be revealed as well, using lattice techniques such as ''cooling'' and alike to help discriminate instantons by their topological charge.

Regarding the applications of our results, we admit that there remains a significant distance to the description of real hadronic processes. Although we hope to cover further phenomenological applications elsewhere, we still would like to comment on two broad but important dynamical issues: (i) the *mechanism of color rearrangements* in high energy collisions and (ii) the issue of *hadronic substructure* of the non-perturbative effects in the hadronic wave functions.

It is generally accepted that high energy hadronic processes can be split into three stages: (i) formation of hadronic wave function (to which we turn later), (ii) color rearrangements of partons in a collision, and (iii) decay of the arising system into multi-hadron final states. It is further believed that at stage (iii) color flux tubes (QCD strings) are formed with basically *unit* probability,[13] so that one can ignore them in the calculation of the cross section. Such assumption is implied in any perturbative approach (such as the Low-Nussinov gluon-exchange model [32]), and we assume that the same is true for instanton-induced color exchanges as well.

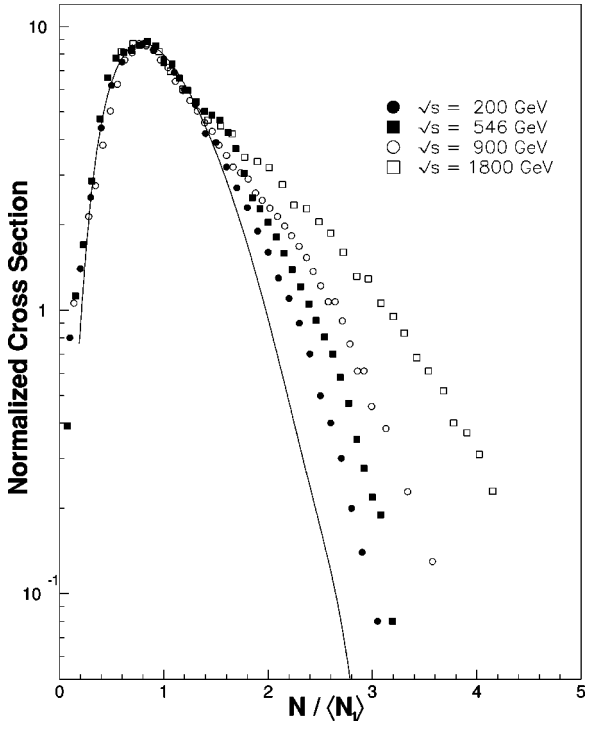

FIG. 9. Multiplicity distribution in $\bar{p}p$ collisions, at 4 different energies from [33]. At each energy the cross section and multiplicity are rescaled, to put the low-*N* part at the universal KNO curve (solid line). This is done to see better the behavior of the ''second component'' discussed in the text.

Our main suggestion for further work is that although the instanton-induced mechanism yields relatively small cross sections, this mechanism is likely to dominate over *events with multiple color rearrangements*. Is there experimental evidence for this assertion in high-energy hadronic collisions? An answer is provided by Fig. 9 (taken from [33]), which shows a (specially normalized) compilation of multiplicity distributions in $\bar{p}p$ collisions at various energies. The data show that there is indeed (at least) two components: (i) one with the cross section $\sigma_1(s)$ and standard Koba-Nielsen-Olesen (KNO) distribution (well known from lower energy pp collisions), as indicated by the solid curve, and (ii) another one with a different cross section $\sigma_2(s)$ and much higher multiplicity. Ascribing the main peak at $N/\langle N_1 \rangle \approx 0.8$ to a *single* color rearrangement reaction (=2 QCD strings formed), one can conclude that at the highest energy $\sqrt{s}=1800$ GeV the multiplicity seen may amount to up to 10 strings.

[13]The fluxes are described by multiple phenomenological models and codes, e.g. the Lund model.

The existence of the second component with double and triple multiplicity was anticipated by physicists doing Regge theory decades ago, in the form of multi-Pomeron exchanges. However, the multiplicity data shown in Fig. 9 do not really fit well into this description. The second component simply does not look as iterations of the first one. There are no separate peaks and, more importantly, the s dependence is completely different. The first component is in fact consistent with the approximation used above, namely an asymptotically constant cross section (zero Pomeron intercept), while the latter grows with $\sqrt{s}$ very strongly.

Attempts to solve this puzzle in PQCD, by summing ladder-type diagrams in leading $\log(x)$ approximation are well known [4], and they do indeed produce strongly growing cross sections and multi-parton states. So the second component may well be due to those perturbative processes. Non-perturbative approaches (aiming mostly at the ''soft Pomeron'' or the first component discussed) have also been tried, from old fashion multi-peripheral hadronic models (e.g. recent work [34]) to mixed gluon-hadron ladders [35,31]. Unfortunately, none of these approaches have lead so far to a quantitative theory.

Results and estimates made in this work lead to the conclusion that instanton-induced color exchanges should dominate over PQCD t-channel gluons starting from the *double* exchange amplitudes. It is therefore logical to conjecture that the second high-multiplicity component of pp collisions may be generated by this mechanism. That would explain why multiple-string events are not just an iteration of the first component, and even consistent with where the transition appears to be. Needless to say that much more work is still needed for a further test of this conjecture.

ACKNOWLEDGMENTS

We thank Maciek Nowak for discussions. This work was supported in part by the U.S. DOE grant DE-FG-88ER40388.

[1] T. Schäfer and E. Shuryak, Rev. Mod. Phys. **70**, 323 (1998).
[2] O. Nachtmann, Ann. Phys. (N.Y.) **209**, 436 (1991); hep-ph/9609365.
[3] A. Muller, Nucl. Phys. **B335**, 115 (1990).
[4] E. Kuraev, L. Lipatov, and V. Fadin, Zh. Éksp. Teor. Fiz. **72**, 377 (1977) [Sov. Phys. JETP **45**, 199 (1977)]; I. Balitskiĭ and L. Lipatov, Yad. Fiz. **28**, 1597 (1978) [Sov. J. Nucl. Phys. **28**, 822 (1978)]; L. Lipatov, Zh. Éksp. Teor. Fiz. **90**, 1536 (1986) [Sov. Phys. JETP **63**, 904 (1986)].
[5] G. Korchemsky, Phys. Lett. B **325**, 459 (1994).
[6] I. Balitsky, Phys. Rev. Lett. **81**, 2024 (1998).
[7] E. Meggiolaro, Nucl. Phys. B (Proc. Suppl.) **64**, 191 (1998).
[8] M. Rho, S. J. Sin, and I. Zahed, Phys. Lett. B **466**, 199 (1999).
[9] R. Janik and R. Peshanski, Nucl. Phys. **B565**, 193 (2000).
[10] A. Ringwald, Nucl. Phys. **B330**, 1 (1990); O. Espinosa, *ibid.* **B343**, 310 (1990).
[11] A. Ringwald and F. Schrempp, hep-ph/9909338.
[12] E. Shuryak, Nucl. Phys. **B203**, 93 (1982); **B203**, 116 (1982); **B203**, 140 (1982); hep-ph/9911244.
[13] H. Casimir and D. Polder, Phys. Rev. **73**, 360 (1948).
[14] M. Peskin, Nucl. Phys. **B156**, 365 (1979).
[15] H. Fujii and D. Kharzeev, Phys. Rev. D **60**, 114039 (1999); hep-ph/9807383.
[16] H. Verlinde and E. Verlinde, hep-ph/9302104.
[17] A. Belavin, A. Polyakov, A. Schwartz, and Y. Tyupkin, Phys. Lett. **59B**, 85 (1975).
[18] G. 't Hooft, Phys. Rev. D **14**, 3432 (1976).
[19] D. Diakonov and Y. Petrov, Nucl. Phys. **B245**, 259 (1984).
[20] T. Hollowood, V. Khoze, and M. Mattis, hep-th/9910118.
[21] E. Shuryak, hep-ph/9909458.
[22] A. Hasenfratz and C. Nieter, Phys. Lett. B **439**, 366 (1998).
[23] C. Callan, R. Dashen, D. Gross, F. Wilczek, and A. Zee, Phys. Rev. **18**, 4684 (1978).
[24] E. Shuryak, Nucl. Phys. **B302**, 574 (1988); D. Chen, R. Brower, J. Negele, and E. Shuryak, Nucl. Phys. B (Proc. Suppl.) **73**, 512 (1999); hep-lat/9809091.
[25] D. Diakonov and V. Petrov, Phys. Lett. B **224**, 131 (1989).
[26] M. Fukushima, H. Suganuma, A. Tanaka, and H. Toki, Nucl. Phys. B (Proc. Suppl.) **63**, 513 (1998); hep-lat/9709133.
[27] T. Schäfer and E. Shuryak, Phys. Rev. Lett. **75**, 1707 (1995).
[28] H. Dosch and Y. Simonov, Phys. Lett. B **205**, 339 (1988); Y. Simonov, Nucl. Phys. **B234**, 67 (1989); O. Nachtmann, Ann. Phys. (N.Y.) **209**, 436 (1991); H. Dosch, E. Ferreira, and A. Krämer, Phys. Rev. D **50**, 1992 (1994); W. Buchmüller, hep-ph/9906546.
[29] M. Good and W. Walker, Phys. Rev. **120**, 1857 (1960).
[30] B. Blättel, G. Baym, L. Frankfurt, H. Heiselberg, and M. Strikman, Phys. Rev. D **47**, 2761 (1993).
[31] E. Shuryak, hep-ph/0001189.
[32] F. Low, Phys. Rev. D **12**, 163 (1975); S. Nussinov, Phys. Rev. Lett. **34**, 1286 (1975).
[33] S. Matinyan and W. Walker, Phys. Rev. D **59**, 034022 (1999).
[34] J. Bjorken, Nucl. Phys. B (Proc. Suppl.) **71**, 484 (1999).
[35] D. Kharzeev and E. Levin, Nucl. Phys. **B578**, 351 (2000).